processes

MDPI

Article

Research on Dynamic Control Methods for Fine-Scale Water Injection Zones Based on Seepage Resistance

Chi Dong [1,2], Weiming Hui [1,2], Gaojun Shan [3], Erlong Yang [2,*], Ming Qu [1,2] and Hai Wang [2]

[1] SANYA Offshore Oil & Gas Research Institute, Northeast Petroleum University, Sanya 572024, China
[2] MOE Key Laboratory of Enhanced Oil Recovery, Northeast Petroleum University, Daqing 163318, China
[3] Daqing Oilfield Co., Ltd., Daqing 163000, China
* Correspondence: yangerlong@nepu.edu.cn

Abstract

To address prominent challenges in developing high water cut oilfields—such as significant variations in sandstone water absorption capacity and uneven reservoir mobilization—this paper proposes a dynamic layered water injection method centered on seepage resistance as the core regulatory indicator. Through theoretical derivation, quantitative relationships are established between seepage resistance, liquid absorption ratio, and injection allocation. Combined with numerical simulation analysis, this forms a refined water injection control strategy that dynamically adjusts according to changes in oilfield water cut. Research findings demonstrate that this method effectively improves fluid absorption profiles in heterogeneous reservoirs, promotes balanced displacement across distinct lithologic zones, and thereby suppresses water cut increase rates and production decline. Taking Block D as an example, maintaining inter-zone seepage resistance step difference within the 3–5 range yields optimal development outcomes. This study provides significant reference value and practical insights for the dynamic development of oilfields in high water cut phases.

Keywords: high-water-cut oilfields; seepage resistance; precision water injection; dynamic regulation

check for updates

Academic Editor: Qingbang Meng

Received: 14 November 2025
Revised: 1 December 2025
Accepted: 4 December 2025
Published: 8 December 2025

Citation: Dong, C.; Hui, W.; Shan, G.; Yang, E.; Qu, M.; Wang, H. Research on Dynamic Control Methods for Fine-Scale Water Injection Zones Based on Seepage Resistance. *Processes* **2025**, *13*, 3966. https://doi.org/10.3390/pr13123966

Copyright: © 2025 by the authors. Licensee MDPI, Basel, Switzerland. This article is an open access article distributed under the terms and conditions of the Creative Commons Attribution (CC BY) license (https://creativecommons.org/licenses/by/4.0/).

1. Introduction

Most developed oil and gas reservoirs in China are continental deposits characterized by significant lateral and vertical heterogeneity. After extensive water flooding, most oilfields have entered the high or ultra-high water cut stage, marked by a highly disordered distribution of remaining oil that is generally scattered but locally concentrated. In the late stage of water flooding, determining the distribution of remaining oil and formulating corresponding production strategies to further enhance oil recovery is a major challenge. The flow field, defined as the dynamic flow path of reservoir fluids, plays a critical role in the distribution of remaining oil. The evolution of the flow field is highly complex and influenced by geological conditions, well patterns, and fluid properties. In some areas, excessive water injection often leads to the formation of dominant flow channels. The uneven distribution of flow fields results in highly dispersed remaining oil and poor efficiency of the water injection process [1]. With the development of the oilfield maturing to the stage of high water cut, the formation pressure field is redistributed, remaining oil becomes increasingly scattered, and fluid properties change throughout the production process, which brings new challenges to the development. For instance, excessive well spacing leads to uneven advancement of injected water in the formation; high-permeability

layers are prone to promoting early water breakthrough, while low-permeability layers suffer from inadequate fluid supply, making them difficult to produce effectively. Interlayer interference has become increasingly prominent, and the difference in water intake capacity between high-permeability and low-permeability layers is several times or even orders of magnitude, which seriously restricts the overall degree of reservoir recovery. In addition, some of the oilfield development well spans hundreds of meters, with thin individual layers and significant variations in physical properties. Therefore, existing well patterns and layer systems struggle to adapt to the dynamic changes in reservoir characteristics, leading to low development efficiency and underutilized recovery potential. Accurately characterizing fluid flow in reservoirs is essential for understanding the fundamental dynamics of multiphase flow, optimizing well patterns, and enhancing oil recovery.

During water flooding, structural fractures, faults, and lateral heterogeneity in permeability often cause rapid advancement of the waterflood front, resulting in ineffective water cycling, low sweep efficiency, and low recovery. Extensive water injection can alter the pore structure and mineral composition of the rock, leading to significant changes in reservoir properties such as porosity, permeability, and wettability [2]. Jiang et al. concluded that variations in reservoir physical properties are generally proportional to the cumulative amount of injected water, and the changes become more pronounced during the high or ultra-high water cut stages [3]. An in-depth study of fluid flow pathways is essential for accurately characterizing the flow field in highly heterogeneous reservoirs during the late stages of water flooding. Flow diagnostic tools can be effectively employed to assess reservoir connectivity and the dynamic evolution of fluid flow paths [4–6]. Compared to full-physics simulations, flow diagnostics offer advantages such as faster computation, greater computational efficiency, and simplified model complexity. As a widely used technique, streamline-based simulation is commonly applied to estimate parameters such as time-of-flight and steady-state tracer distributions [7–10]. Additionally, flow heterogeneity has been characterized by introducing specific parameters, including swept regions, drainage areas, well-pair regions, and the Lorenz coefficient, which help describe flow dynamics within the reservoir. Thiele and Batycky used streamline-based simulation to calculate flow rates between well pairs and derived optimal injection–production parameters [11]. Jia and Deng developed a flow field identification method based on streamline simulation, and they analyzed streamline bundles to identify areas of ineffective water cycling via Python3.10 programming [12]. Tanaka et al. combined streamline-based simulation with a genetic algorithm to generate preliminary development plans [13]. They integrated this approach with response surface methodology to derive an optimal strategy for a typical waterflooded reservoir, significantly reducing model complexity. Zhao Chunsen et al. analyzed the factors affecting water flooding efficiency using numerical simulation technology [14]. Zhang et al. developed a comprehensive geological model, designed and compared multiple water injection schemes, and successfully quantified the negative impact of reservoir heterogeneity on water flooding performance [15]. They demonstrated that refined water injection strategies, especially those combining dynamic adjustments with intelligent distributed injection, can effectively mitigate these adverse effects, thereby significantly enhancing both recovery and economic benefits. Ultimately, they proposed a set of dynamic optimization strategies. Wang et al. developed an intelligent system to address the challenges of layered water injection in highly heterogeneous, multilayer sandstone oilfields during the high water cut stage [16]. This system integrates surface control, downhole tools, and software to enable real-time monitoring and remote precise regulation of parameters such as flow rate, pressure, and temperature in each injection layer, significantly enhancing the efficiency of layered water injection. Sun et al. proposed and validated an innovative bridge-type concentric layered water injection system [17]. This system enables long-term,

continuous monitoring of individual tubing pressures and downstream pressures at each layer during conventional water injection, providing essential data for dynamic analysis. Song et al. introduced layered flow-allocation technology for water injection wells based on wave-code communication, accelerating the advancement toward intelligent management of injection wells [18]. This technology is expected to drive the field of refined layered water injection toward greater intelligence, automation, and integration [19]. As the field water cut continues to grow, the driving mechanism behind interlayer conflict has shifted from being "static-dominated" to involving "static-dynamic coupling". During the early development stage, interlayer interference was primarily governed by static geological factors such as permeability, sand thickness, and porosity. However, upon entering the high water cut stage, the flow resistance of fluids within individual sublayers exhibits significant differential variations as water cut increases. In high-permeability layers, intensified water flooding leads to increased water saturation, which reduces flow resistance and further enhances water intake capacity, creating a vicious cycle of "water theft" [20,21]. In contrast, low-permeability layers experience a marked increase in flow resistance due to elevated oil viscosity and bound water clogging pore throats, resulting in a continuous decline in water intake capacity. At this stage, interlayer interference is no longer solely the result of static factors but rather arises from the coupling of static reservoir properties and dynamic development parameters. Traditional layer adjustment methods based solely on static parameters can no longer meet the requirements of precision development.

In this context, our objective is to develop a novel dynamic control method for layered water injection based on seepage mechanics theory. This method utilizes a quantitative flow resistance calculation model that integrates both static and dynamic parameters between injectors and producers [22]. It can accurately characterize the flow paths and resistance distribution across different layers between injection and production wells, enabling dynamic evaluation of the production potential of each layer and providing more targeted adjustment strategies for oilfield development. This study focuses on developing a dynamic control methodology for layered water injection and systematically undertakes the following tasks: First, based on a comprehensive diagnosis of developmental challenges in the target block, the principle of hydraulic similarity is applied to quantitatively characterize the flow resistance of individual layers. Corresponding evaluation criteria are established to verify its correlation with the sandstone's water intake capacity. By optimizing the flow resistance differential between layers, a theoretical foundation is provided for rational layer combination and partitioning. Furthermore, by deriving the quantitative relationship between flow resistance and injection allocation rates using the two-phase Darcy's Law and analyzing the dynamic impact of flow resistance variations on injection allocation across different water cut stages, an optimized water injection strategy is formulated. Finally, the maximum potential for enhanced oil recovery that is achievable through this method is determined.

2. Problem Statement

Block D was initially developed using a reverse nine-spot pattern with a well spacing of 300 m. It was divided into four reservoir units, developed with three sets of well patterns. In the central area of Block D, where the reservoir is thicker, two well patterns were deployed: one for the Gaoyi I and II reservoir units and another for the Gaoyi III and IV reservoir units, targeting the GI1–II25 and GII26-and-below reservoirs, respectively. A 300 m five-spot pattern was used for GI1–GI20, a 212 m five-spot pattern was used for GII1–GII34, and a 300 m reverse nine-spot pattern was used for GII26–GIV1. The average reservoir permeability in Block D is 231 mD, porosity is 26%, average oil saturation is 59.5%, surface crude oil density is 0.865 g/cm^3, and formation crude oil viscosity is 9.2 mPa·s.

Based on continuous water injection profile data from recent years, the overall displacement efficiency in Block D is moderate. The proportion of poorly displaced and non-displaced sandstone reaches 51.7%, while the proportion of effective thickness accounts for 47.5%. Poorer reservoir properties correlate with worse development performance. For reservoirs with an effective thickness greater than 1.0 m, the proportion of poorly developed and undeveloped sandstone is 38.6%. However, for reservoirs with an effective thickness less than or equal to 1.0 m and with extra-reservoir oil layers, the proportion reaches 55.0%. This indicates that under the current well pattern, reservoir adaptability is poor and development efficiency is low. Although refined layered water injection has improved the utilization status in Block D in recent years, significant disparities in utilization levels persist across different reservoir types.

Currently, some formations in Block D have low residual oil saturation, leading to reduced flow resistance. Reservoirs with poor utilization have a low water cut and high residual oil saturation, which further exacerbates the differences in flow resistance between formations. This paper presents an investigation into the dynamic regulation of the GI1-GI20 formation series, utilizing a representative model of Block D and employing seepage resistance as the foundational criterion.

3. Seepage Resistance Calculation Model

As shown in Figure 1, the seepage resistance method utilizes the principle of hydraulic similarity to describe the relationship between flow rate and permeability in reservoir seepage fields by drawing an analogy to current and resistance in electrical circuits [23] (assuming it is a radial flow, and the oil–water two-phase process is incompressible, and the density does not change with pressure). In practical applications, the workflow primarily focuses on well groups centered around water injection wells. Based on the dynamic and static development parameters of these well groups, seepage resistance coefficients under two-phase flow conditions are calculated for individual layers or segments of both producer and injector wells.

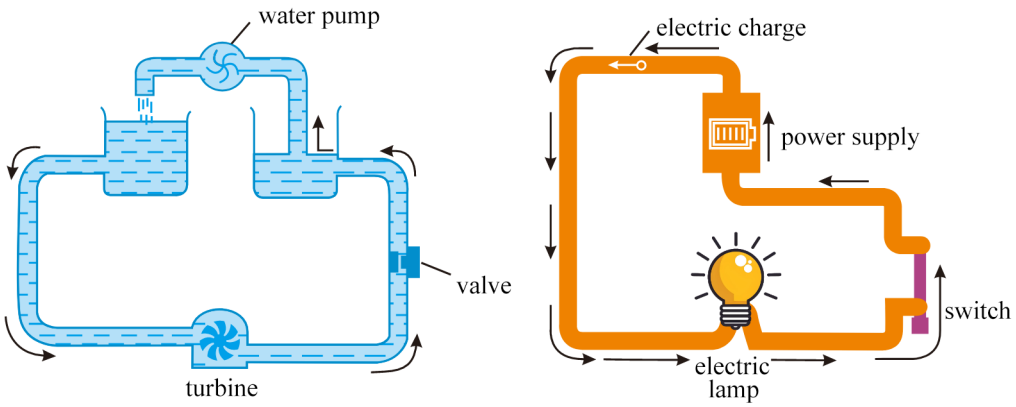

Figure 1. Schematic diagram of similar principles in hydropower and electricity processes.

According to Darcy's Law, it can be seen that the flow resistance of the oil and water phases in the reservoir is related to the water saturation function, the viscosities of the oil and water phases, the relative permeability, and the well spacing between oil and water wells.

Two-Phase Flow Conditions for Darcy's Equation:

$$Q = KA\left(\frac{K_{ro}(S_w)}{\mu_o} + \frac{K_{rw}(S_w)}{\mu_w}\right)\frac{\Delta P}{L} \quad (1)$$

Equivalent seepage resistance:

$$R = \frac{\Delta P}{Q} = \frac{1}{\frac{KK_{ro}(S_w)}{\mu_o} + \frac{KK_{rw}(S_w)}{\mu_w}} \frac{L}{A} \quad (2)$$

where Q is flow rate, m^3/s; K is absolute permeability, mD; A is rock cross-sectional area, m^2; S_w is water saturation, %; K_{ro} is oil phase relative permeability; K_{rw} is water phase relative permeability; μ_o is crude oil viscosity, mPa·s; μ_w is water viscosity, mPa·s; P is pressure gradient, Pa; and L is flow distance, m.

During field application, the approximate calculation method for the seepage resistance coefficient is as follows.

Within the injection–production well group, the seepage resistance between wells in a single direction within the sub-formation is first calculated. Subsequently, based on the principle of the hydraulic–electrical analogy, the planar seepage resistance of the sub-formation is determined [24,25].

Seepage resistance at any point along the main flow path between oil and water wells:

$$R(x) = \frac{1}{K(x)h(x)(K_{ro}/\mu_o + K_{rw}/\mu_w)} \quad (3)$$

where $R(x)$ represents the inter-well flow resistance, $mPa{\cdot}s{\cdot}mD^{-1}{\cdot}m^{-1}$; $K(x)$ denotes the permeability at any point along the main flow path between oil and water wells, mD; and $h(x)$ indicates the thickness at any point along the main flow path between oil and water wells, m.

Calculate the flow resistance in a single layer of an injection well along a specific injection–production direction:

$$R_i = \int_{r_w}^{d} R(x)\mathrm{d}x \quad (4)$$

where d is the distance between oil and water wells, m, and r_w is the wellbore radius, m.

Through segmented discretization and summation between oil and water wells, the single-layer flow resistance is the sum of flow resistances from the injection well to each production well. Since a single production–injection well connects multiple injection–production directions (i.e., n production wells), it is equivalent to n resistors in parallel on the plane. Thus, the flow resistance on the mth sublayer is as follows:

$$R_m = \frac{1}{1/R_1 + \cdots + 1/R_i + \cdots + 1/R_n} \quad (5)$$

This article selects a small typical small block from a whole region model, which has a good historical fit and high accuracy. Determine the main flow paths between oil and water wells in different stratigraphic zones based on the stratigraphic well network flow diagram (Figures 2 and 3) to facilitate subsequent calculation of stratigraphic flow resistance. The calculation process is illustrated in Figure 4.

Using the aforementioned process, the flow resistance of each sublayer within the stratum was calculated. The wellbore radius is 0.14 m, crude oil viscosity is 9.2 mPa·s, and water viscosity is 1 mPa·s. The calculation results are presented in Table 1. The data in Table 1 can indicate the differences in seepage resistance among different layers, which are mainly due to the different pore structures, permeability, and throat radii of each layer. Moreover, changes in water saturation dynamically alter the seepage resistance of each phase fluid through the relative permeability effect, resulting in significant differences in seepage resistance among different sub layers.

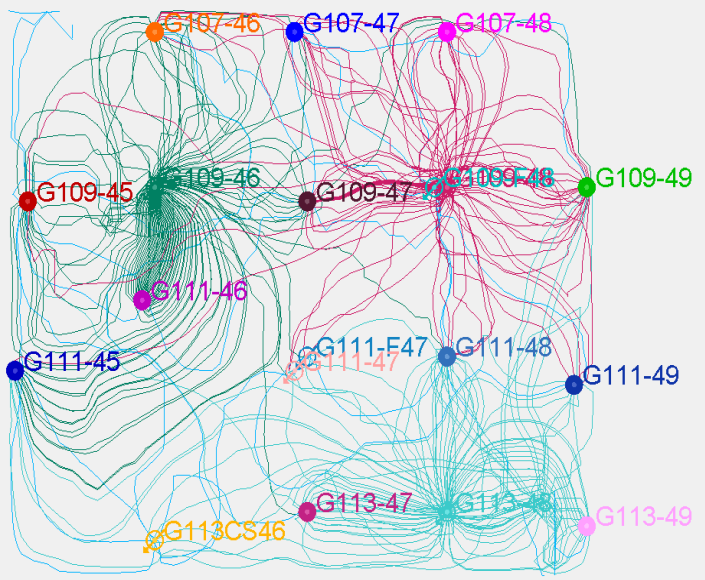

Figure 2. Flowline diagram of Block D well network.

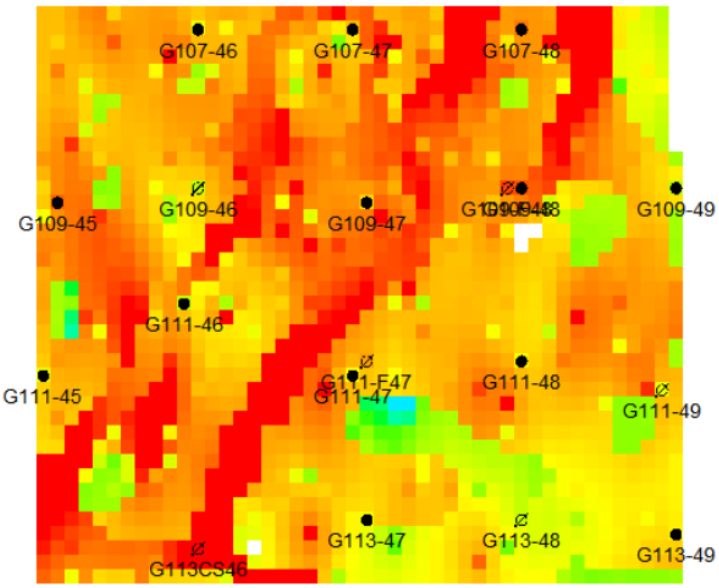

Figure 3. Block D well location map.

Table 1. Initial flow resistance of sublayers in stratigraphic Series GI1–GI20.

Layer	Seepage Resistance, mPa·s·mD^{-1}·m^{-1}	Layer	Seepage Resistance, mPa·s·mD^{-1}·m^{-1}	Layer	Seepage Resistance, mPa·s·mD^{-1}·m^{-1}
G11	12.51	G110	5.34	G116	1.13
G12+3	7.11	G111	2.61	G117	0.31
G14+5	4.05	G112	1.22	G118	1.50
G16+7	6.19	G113	1.42	G119	0.34
G18	8.47	G114	1.45	G120	0.62
G19	2.92	G115	0.52	/	/

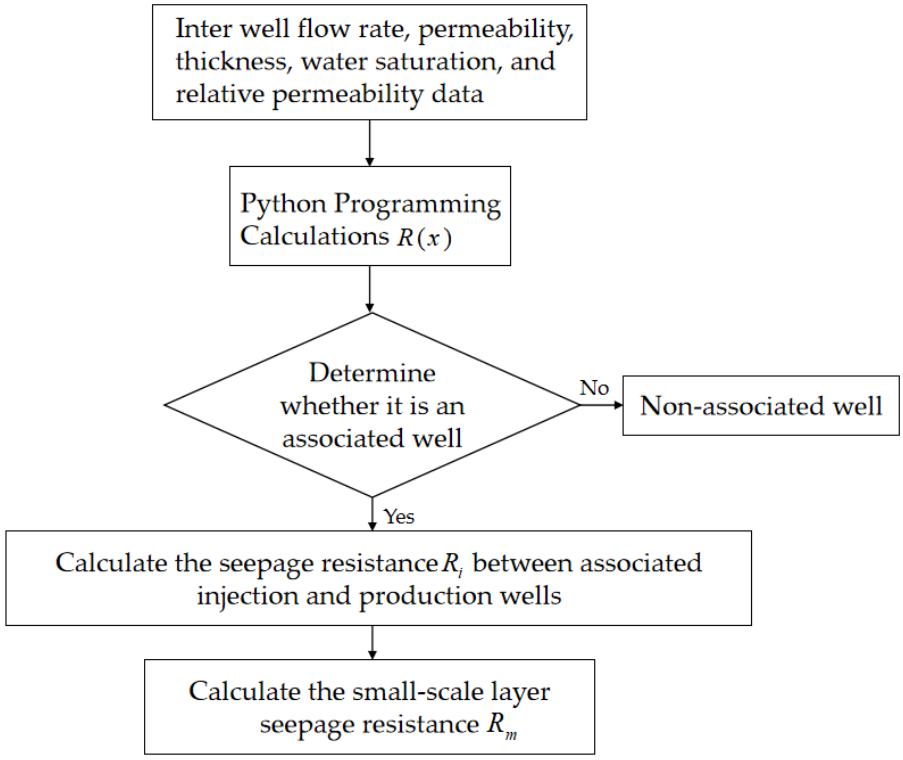

Figure 4. Flowchart of permeability resistance in the computational layer.

4. Establish Criteria for Determining Seepage Resistance

By integrating reservoir numerical simulation with injection well test data (sandstone thickness and effective thickness data are obtained from actual well logging data, and the sandstone liquid absorption ratio is obtained from numerical simulation model production PRT files), a feasibility analysis of flow resistance was conducted based on the aforementioned flow resistance calculation results. A total of 17 flow resistance values across 6 injection wells in the study block were calculated and statistically analyzed. The sandstone thickness is 22.57 m, with an effective thickness of 10.11 m and a single-cycle sandstone water absorption ratio of 31.58%. Comparing the single-cycle sandstone water absorption ratios, the mobilization ratio progressively increases with rising flow resistance. As shown in Table 2, when flow resistance exceeds 10 mPa·s/(mD·m), the single-cycle sandstone water absorption ratio decreases from 35.67% to 23.6%. This indicates a strong correlation between the reservoir's hydraulic resistance coefficient and the water absorption mobilization status of sandstone in the reservoir. Higher hydraulic resistance correlates with lower mobilization levels.

Table 2. Water absorption proportion of sandstone with different seepage resistance.

Seepage Resistance Zone ($mPa{\cdot}s{\cdot}mD^{-1}{\cdot}m^{-1}$)	Number of Floors	Sandstone Thickness (m)	Effective Thickness (m)	Sandstone Water Absorption Ratio (%)
0–5	12	14.79	5.91	35.67
5–10	4	6.42	3.49	30.89
>10	1	1.37	0.71	23.6
Total	17	22.57	10.11	31.58

Using the Eclipse2020(Schlumberger, Houston, Texas, USA) numerical simulation software, a numerical simulation model was established. Low-permeability combinations (50 mD and 100 mD), medium-permeability combinations (100 mD and 200 mD), and high-permeability combinations (500 mD and 1000 mD) were designed for simulations

(Figure 5). Two small layers with the same permeability differential but different permeability combinations were simulated in parallel for displacement to investigate interlayer interference. As the water cut increases, the oil phase permeability decreases while the water phase permeability increases. The ratio of flow resistance between the two layers gradually rises. When the water cut exceeds 70%, this ratio begins to increase gradually, while the ratio of flow resistance between the two layers increases sharply if the water cut surpasses 90%. The flow velocity of injected water in the small layer increases, and the interlayer conflict becomes more pronounced, as shown in Figures 6 and 7.

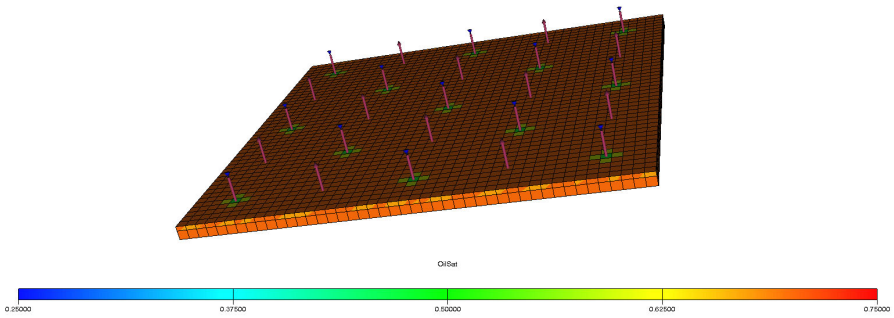

Figure 5. Ideal model of interlayer interference patterns.

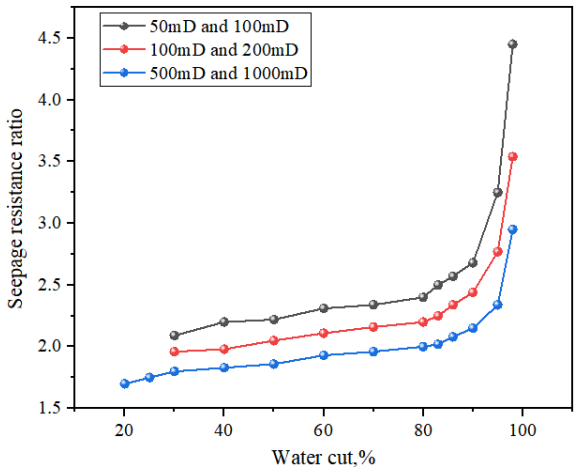

Figure 6. Ratio of interlayer seepage resistance for different permeability combinations as a function of water cut.

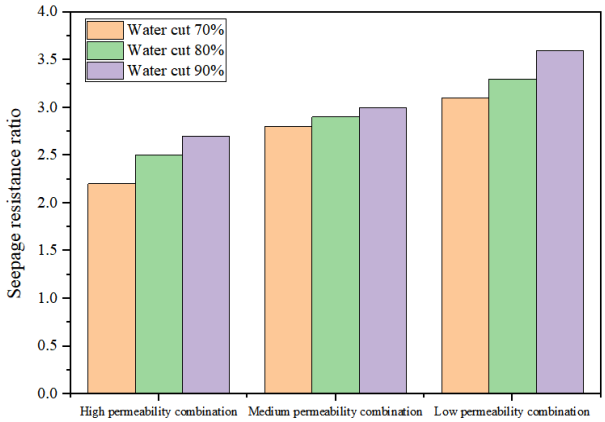

Figure 7. Interlayer seepage resistance ratio for different permeability combinations at various water cut levels.

In summary, during the low-to-medium water cut period, static heterogeneity controlled by physical properties is the primary factor governing interlayer, planar, and intralayer conflicts in oilfield development. Following long-term water injection development, small layers with identical permeability exhibit significant variations in water saturation, leading to changes in flow resistance. At this stage, permeability differences fail to reflect fluid flow variations within the reservoir, whereas flow resistance exhibits dynamic characteristics that directly reflect the flow state of small layers. Currently, field-based stratigraphic unit delineation combines reservoirs with similar properties under the premise of sufficient reserve abundance within each unit. This approach primarily considers static indicators such as the permeability coefficient variation within reservoirs, perforated sandstone thickness within sections, and the number of perforated reservoirs. However, based on flow characteristics during high water cut periods, relying solely on static indicators for stratigraphic grouping fails to precisely characterize flow changes during high water cut phases. Therefore, a stratigraphic adjustment method centered on dynamic flow resistance as the primary indicator must be established.

5. Research on Dynamic Regulation Methods for Layer Segments

5.1. Optimal Gradient for Seepage Resistance

To determine the appropriate seepage resistance differential for precise water injection control, seven stratigraphic combinations were designed based on the seepage resistance step difference values of each minor stratum from the numerical simulation model of the actual block. This establishes the differential range for inter-stratum seepage resistance combinations during stratigraphic adjustments. The design proposals are presented in Table 3.

Table 3. Interlayer seepage resistance gradient scheme.

Interlayer Seepage Resistance Gradient	Recovery Rate, %
1.11	25.49
2.66	27.10
3.4	28.72
4.93	33.76
8.14	28.47
9	27.48
11.82	20.16

By optimizing the permeability gradient, it is found that a gradient range between 3.4 and 4.93 significantly enhances reservoir recovery rates (Figure 8). In contrast, gradients that are either too low or too high have a relatively weaker impact on reservoir recovery rates. This occurs because a small gradient promotes uniform fluid injection without natural differentiation. However, once a main flow path forms, the uniform leading edge of the displacement fluid tends to cause overall synchronous flooding, making it difficult to further increase the sweep efficiency. Conversely, an excessively large gradient results in low natural sweep efficiency and increased flow leakage, preventing recovery improvement or even causing it to decline.

Therefore, the intralayer permeability gradient should be controlled within the range of 3 to 5 when defining subsequent stratigraphic combinations.

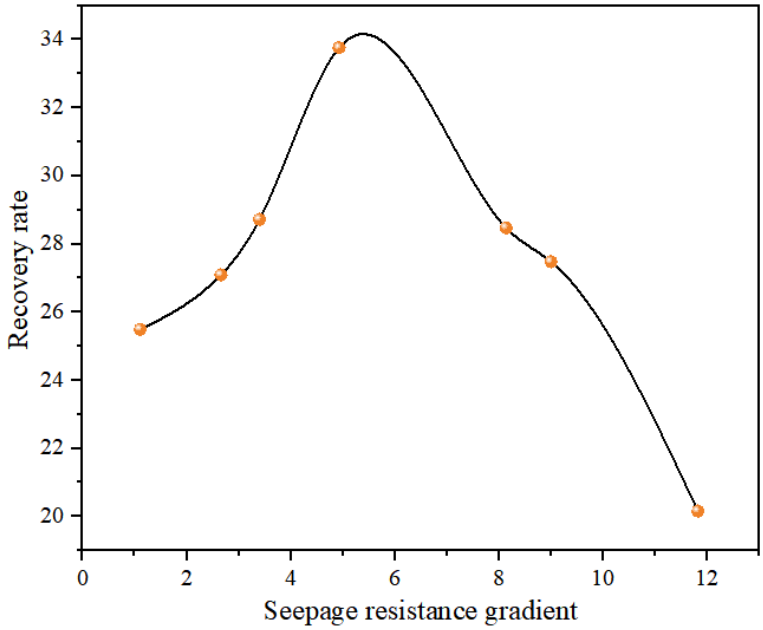

Figure 8. Relationship between seepage resistance gradient and recovery rate.

5.2. The Relationship Between Liquid Absorption Ratio and Seepage Resistance

Through continuous variation in interlayer seepage resistance during development, layer-segment combinations were optimized and layered water injection implemented to mitigate uneven seepage resistance. To define the technical boundaries for layered water injection during high water cut periods, a mechanistic model was employed to investigate the variation patterns of seepage resistance coefficients and their impact on interlayer interference. An idealized model was established featuring three longitudinally heterogeneous layers with plane-homogeneous properties, equal interlayer thicknesses, and boundary conditions simulating steady-state production with injection–production balance. A comprehensive seepage resistance model was employed to calculate the integrated seepage resistance coefficients for low-, medium-, and high-permeability layers (100 mD, 300 mD, and 600 mD), along with layer-specific liquid absorption patterns. The variation in seepage resistance coefficient across different water cut levels was statistically analyzed.

Figures 9 and 10 demonstrate that the water saturation of the high-permeability layer rises rapidly as water cut increases, leading to a rapid decrease in seepage resistance within the layer and consequently increasing liquid uptake. The disparity in liquid uptake ratios among low-, medium-, and high-permeability layers initially narrows, but upon reaching the high water cut stage, the difference in uptake ratios significantly widen. The coefficient of variation in flow resistance across the three-layer model gradually increases with rising water content. The variation in seepage resistance between layers becomes markedly pronounced when water cut exceeds 60%. Therefore, layered water injection should be employed if seepage resistance differences between layers are significant. Layered injection parameters must adapt to changes in water cut stages, and dynamic parameter variations must be considered during implementation.

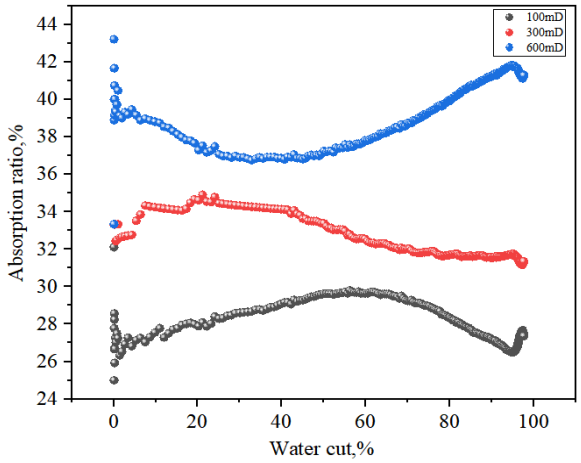

Figure 9. Liquid absorption ratio by layer in the three-layer model.

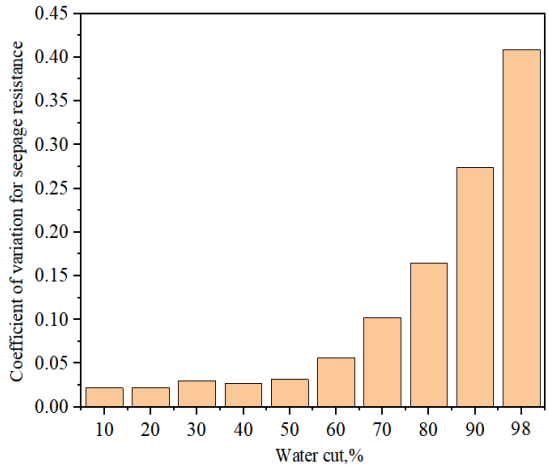

Figure 10. Variation coefficient of seepage resistance in the three-layer model.

5.3. Water Injection Control Strategy

The specific dynamic regulation strategy for layer intervals establishes a multi-parameter decision-making framework. The seepage resistance distribution determines the overall direction of injection adjustments, with spatial variations guiding whether injection rates in individual layers should increase or decrease. The characteristic water cut stage governs the frequency of dynamic regulation; the adjustment frequency increases during high water cut stages and appropriately decreases during low water cut stages. Static parameters, such as effective thickness and permeability, define the safe operational boundaries for injection rates, ensuring that adjustments remain within the reservoir's capacity and effectively prevent formation damage caused by over-potential injection. First, assume that each sublayer within the same water injection well constitutes a parallel flow unit, with the fluid being incompressible. The flow within each sublayer follows Darcy's Law for two-phase flow. For oil–water two-phase flow, the oil phase flow rate Q_o and water phase flow rate Q_w are combined with an extension of Darcy's Law, yielding effective permeability coefficients Ki for the oil phase and water phase as KK_{ro} and KK_{rw}, respectively.

Darcy's Law for Oil Phase:

$$Q_o = \frac{K \cdot K_{ro} \cdot h_i \cdot \Delta P}{\mu_o \cdot L} \tag{6}$$

Darcy's Law for the Aqueous Phase:

$$Q_w = \frac{K \cdot K_{rw} \cdot h_i \cdot \Delta P}{\mu_w \cdot L} \tag{7}$$

The total flow rate Q_i of the laminar flow is obtained by adding the oil phase flow rate Q_o and the water phase flow rate Q_w:

$$Q_i = Q_o + Q_w = \frac{K \cdot K_{ro} \cdot h_i \cdot \Delta P}{\mu_o \cdot L} + \frac{K \cdot K_{rw} \cdot h_i \cdot \Delta P}{\mu_w \cdot L} \tag{8}$$

After organizing, we obtained the following:

$$Q_i = \frac{K_i \cdot h_i \cdot \Delta P}{\frac{\mu_o \cdot L}{K_{ro}} + \frac{\mu_w \cdot L}{K_{rw}}} \tag{9}$$

The definition equation for small-layer seepage resistance is $R_L = \frac{\Delta P}{Q_i}$.

From this, we derive the definition equation for seepage resistance as follows:

$$R_L = \frac{L}{K_i \cdot h_i}\left(\frac{\mu_o}{K_{ro}} + \frac{\mu_w}{K_{rw}}\right) \tag{10}$$

Substituting Equation (10) into Equation (9) yields the fundamental relationship between the injection rate and the seepage resistance.

$$Q_i = \frac{\Delta P}{R_L \cdot L_i} \tag{11}$$

When the injection–production pressure differential ΔP and the injection–production well spacing L are fixed, a higher reservoir flow resistance R_L results in a smaller proportionate injection rate Q_i, preventing "under-injection" in high-permeability resistive zones. Conversely, a lower R_L leads to a larger Q_i, suppressing "water-grabbing" in low-permeability resistive zones.

The individual aquifers within the same injection well exhibit parallel flow, with the total fluid intake for the entire well being $Q_{Total} = \sum_{i=1}^{n} Q_i$. Combined with (11), the fluid absorption ratio $f_i = \frac{Q_i}{Q_{Total}}$ can be further derived as $f_i = \frac{\frac{\Delta P}{R_L \cdot L_i}}{\sum_{L=1}^{n} \frac{\Delta P}{R_L \cdot L_i}}$. With wells in the same well group having approximately similar distances, the relationship between the fluid absorption ratio and the flow resistance can be obtained after consolidation.

$$f_i = \frac{1/R_L}{\sum_{L=1}^{n} 1/R_L} \tag{12}$$

The wicking ratio f_i is inversely proportional to the seepage resistance R_L.

In order to prevent excessive water injection pressure from fracturing reservoir rocks and causing irreversible damage, the bottomhole flow pressure must be lower than the formation fracture pressure:

$$P_{wf} \leq P_{frac} \tag{13}$$

The bottomhole flowing pressure is related to wellhead pressure, static fluid column pressure, etc. For injection wells, the injection–production pressure difference ΔP can be

approximately expressed as the difference between the bottomhole flowing pressure and the average reservoir pressure P_{avg}:

$$\Delta P = P_{wf} - P_{avg} \tag{14}$$

By substituting the above equation into the fracture pressure constraint condition, we obtain the safe upper limit of the injection–production pressure difference:

$$\Delta P_{\max} = P_{frac} - P_{avg} \tag{15}$$

By substituting the maximum allowable pressure difference into Equation (11), the maximum safe injection quantity Q_i^{frac} for a single layer based on formation integrity can be obtained as follows:

$$Q_i^{frac} = \frac{\Delta P_{\max}}{R_i \cdot L} = \frac{P_{frac} - P_{avg}}{R_i \cdot L} \tag{16}$$

Even if the injection–production pressure difference is within a safe range, the injection volume of a single layer should not exceed its inherent potential. We can establish another upper limit of injection quantity $Q_i^{potential}$, which is proportional to the average reservoir pressure (representing the energy level of the formation) and the reservoir potential coefficient:

$$Q_i^{potential} = \lambda_i \cdot f(P_{avg}) \tag{17}$$

Among them, $f(P_{avg})$ is a function related to the average reservoir pressure, used to correct the influence of formation energy on water absorption capacity (for example, the lower the energy, the greater the potential space for injection, but the relationship may be nonlinear).

For any regulatory layer, the final injection quantity Q_i^{final} must satisfy both Equations (18) and (19) simultaneously:

$$\Delta P < \Delta P_{\max} = P_{frac} - P_{avg} \tag{18}$$

$$Q_i < Q_i^{potential} = \lambda_i \cdot f(P_{avg}) \tag{19}$$

Therefore, the complete mathematical expression for safe dosing is as follows:

$$Q_i^{final} = \min\left(\frac{P_{frac} - P_{avg}}{R_i \cdot L}, \lambda_i \cdot f(P_{avg}), Q_i\right) \tag{20}$$

In the above equation, P_{wf} is the bottomhole flowing pressure, MPa; P_{frac} is the formation fracture pressure, MPa; P_{avg} is the average reservoir pressure, MPa; and λ_i is the reservoir potential coefficient.

In practical regulation, the seepage resistance R_L of each layer is first calculated using Equation (10), and then the theoretical liquid absorption ratio f_i of each layer is calculated using Equation (12). This formula clearly states that the layer with lower seepage resistance should have a lower theoretical liquid absorption ratio; on the contrary, layers with high seepage resistance should have a higher water injection ratio to suppress layer interference. Based on the total injection volume Q_{Total} of the entire well, calculate the theoretical injection volume Q_i of each layer. Calculate the maximum safe injection volume Q_i^{frac} of a single layer based on the formation fracture pressure according to Equation (16), and then estimate the maximum injection volume $Q_i^{potential}$ of the reservoir potential limit by combining the static parameters of the reservoir (such as effective thickness and permeability) according to Equation (17). Finally, calculate Q_i^{final} based on the safety injection volume constraint conditions of Equation (20). In practical regulation, regulation is not a one-time process,

but a cyclical process that changes dynamically with the development of the oilfield. The adjustment period in the early stage of high water cut is usually set at 1–3 months. By dynamically adjusting the seepage resistance of each layer through the influence of different water cut phases on the liquid absorption ratio of each layer, the dynamic control effect can be achieved.

When in the actual regulation process, with the change in seepage resistance, the difference in seepage resistance between layers exceeds the optimal range of 3–5, and the layers are recombined to ensure that each layer is within a reasonable range of seepage resistance difference, and the injection volume also changes accordingly.

6. Practical Application

This article adopts a multi-stage isolation system for layered water injection, with multiple isolation devices installed inside each water injection well to ensure that the water flow in each layer does not interfere with each other during the water injection process. After calculating the injection volume of each layer through a formula, layer-by-layer water injection is carried out, and fine water injection is carried out by plugging other layers while injecting water into the injection layer. Firstly, a numerical simulation model is used to study the dynamic regulation of layered water injection based on seepage resistance at different water content times according to the layered water injection scheme.

Taking the actual model of Block D as an example. The stratum G11–G120 was fully perforated and produced, with a five-point well network comprising 6 injection wells and 13 production wells. Formulas were derived to calculate the relationship between seepage resistance, liquid absorption ratio, and injection allocation for the sublayer. A zoned injection scheme was designed based on seepage resistance differentials for various water cut scenarios, contrasting it with a blanket injection approach. Eclipse software was employed for scheme prediction, with projected recovery rates presented in Appendix A, Table A1. See Figures 11 and 12 for the prediction effect of the scheme.

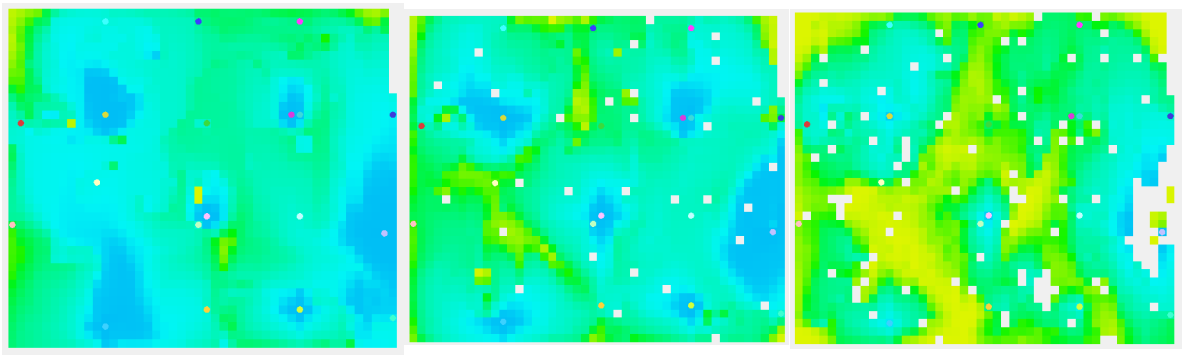

(**a**) Fifth Level (**b**) Nineteenth Level (**c**) Thirty-first Level

Figure 11. Oil saturation map for selected sublayers in the original plan.

The stage recovery rate for the general water injection method is 28.11%. Starting from a water cut of 70%, predict the recovery rate and implement layered water injection based on the flow resistance of different zones at various water content levels. As shown in Figure 13, the effectiveness of zoned injection diminishes as water cut increases. Between 70% and 78% water cut, zoned injection based on gradient flow resistance yields optimal results, achieving a maximum recovery rate increase of 3.97% (See Appendix B for the benefit analysis of this plan). However, the advantage of zoned injection significantly declines if water cut exceeds 80%, and no further improvement in recovery is observed when water cut exceeds 90%.

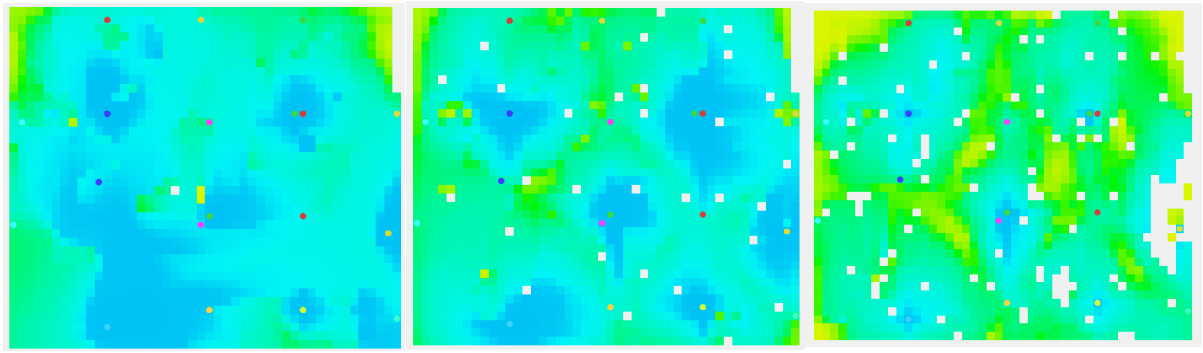

(**a**) Fifth Level (**b**) Nineteenth Level (**c**) Thirty-first Level

Figure 12. Oil saturation in small layers during staged water injection at 70% water cut.

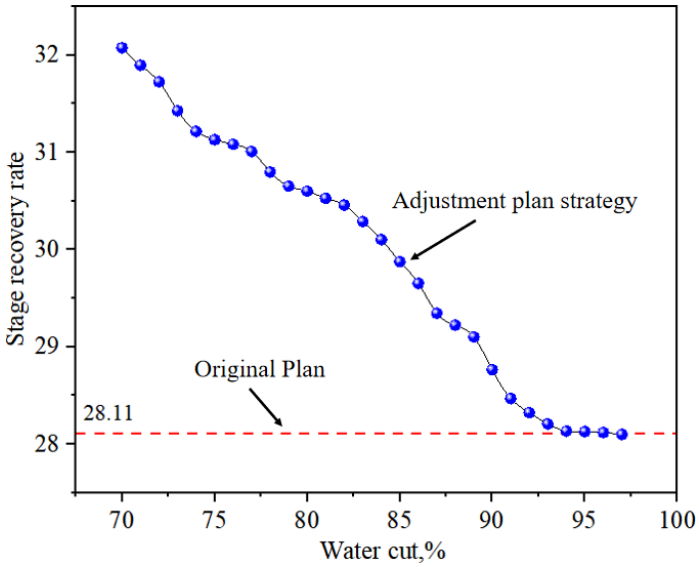

Figure 13. Recovery rate during staged water injection at different water content levels.

Fluid flow resistance is low in high-permeability layers. If not controlled appropriately, injected water will preferentially flow rapidly through these high-permeability zones, causing further erosion and enlargement of their pore channels. This means that a significant portion of injected water will be ineffectively circulated during the development stage without early intervention, failing to efficiently drive crude oil in low-permeability layers. Therefore, implementing early-stage layered water injection—where the injection rate in smaller layers is matched to the permeability of high-permeability zones—effectively enhances displacement pressure in low-permeability layers. This accelerates the development of low-permeability zones, maximizing the vertical utilization of the reservoir. When the moisture content is greater than 90% and the interlayer seepage resistance is controlled within the range of 3–5, there is no significant increase in recovery rate, and a decrease in recovery rate may even occur, compared to the medium to high moisture content period. The core reason for the decrease in recovery rate is that the main contradiction in development has changed. The differential control of seepage resistance is an extremely effective technique for improving macroscopic sweep efficiency and tapping interlayer potential, but its effectiveness is limited by two more fundamental physical and geological conditions: low micro displacement efficiency and insufficient movable oil saturation in the ultra-high water cut stage. To further improve the recovery rate at this stage, it is often necessary to turn to more powerful methods such as chemical or gas flooding to change the flowability ratio and interfacial tension, thereby improving the micro displacement efficiency.

7. Conclusions

Based on the dynamic evolution characteristics of seepage resistance, this study proposes an integrated, refined layered water injection methodology tailored for high water cut reservoirs. The results demonstrate that seepage resistance, as a dynamic characterization parameter, more accurately describes fluid seepage patterns in reservoirs during high water cut stages. This approach effectively overcomes the limitations of traditional static parameters and offers a novel technical solution for efficient oilfield development. The main findings are as follows:

(1) The coefficient of variation in seepage resistance exhibits a significant positive correlation with water cut. When the water cut exceeds 70%, the coefficient increases sharply, indicating that static analysis methods based on permeability differences can no longer accurately characterize the actual flow behavior within the reservoir. In contrast, seepage resistance, due to its dynamic response characteristics, more directly reflects the true flow conditions of individual sublayers.

(2) By integrating the two-phase Darcy's Law with the water-electricity analogy principle, a practical calculation model for the seepage resistance coefficient was developed. Using a self-developed algorithm, the study quantitatively characterized layer seepage resistance. It determined that the optimal range for the seepage resistance step difference, used as a layering criterion, is 3–5, thereby providing a scientific basis for optimizing layer combination.

(3) An innovative, refined water injection control method based on the dynamic characteristics of seepage resistance was proposed. This method dynamically optimizes layered water injection strategies by monitoring real-time changes in seepage resistance, significantly enhancing the accuracy and responsiveness of injection control.

(4) The effectiveness of layered water injection is significantly influenced by the water cut. Experimental data show that within the water cut range of 70% to 78%, the injection strategy guided by seepage resistance differential achieves optimal results, with a projected recovery increase of 3.97 percentage points. This approach offers an effective means of enhancing production in high water cut oilfields.

This study confirms the superiority of flow resistance in characterizing the dynamic properties of high water cut reservoirs. The developed dynamic control method offers new technical support for enhancing the development efficiency of these reservoirs.

Author Contributions: Conceptualization, C.D.; investigation, G.S.; writing—original draft, W.H.; writing—review and editing, E.Y., M.Q., and H.W. All authors have read and agreed to the published version of the manuscript.

Funding: The research was supported by the Hainan Provincial Joint Project of Sanya Yazhou Bay Science and Technology City, Grant (No:2021JJLH0059), and Heilongjiang Postdoctoral Fund (LBH-Z23105).

Data Availability Statement: The original contributions presented in this study are included in the article. Further inquiries can be directed to the corresponding author.

Conflicts of Interest: Author Gaojun Shan was employed by the company Daqing Oilfield Co., Ltd. The remaining authors declare that the research was conducted in the absence of any commercial or financial relationships that could be construed as a potential conflict of interest.

Appendix A

Table A1. Layered water injection plan at different water content levels.

Water Cut, %	Layer-Segment Combination	Seepage Resistance Gradient	Stage Recovery Rate, %
70	G11–G18	2.80	32.075
	G19–G111	2.04	
	G112–G116	2.79	
	G117–G120	4.68	
71	G11–G18	2.77	31.896
	G19–G111	2.05	
	G112–G116	2.78	
	G117–G120	4.67	
72	G11–G18	2.77	31.724
	G19–G111	2.06	
	G112–G116	2.77	
	G117–G120	4.68	
73	G11–G18	2.89	31.428
	G19–G111	2.07	
	G112–G116	2.75	
	G117–G120	4.69	
74	G11–G18	3.33	31.215
	G19–G111	2.09	
	G112–G116	2.73	
	G117–G120	4.71	
75	G11–G18	3.55	31.131
	G19–G111	2.10	
	G112–G116	2.72	
	G117–G120	4.73	
76	G11–G18	3.60	31.082
	G19–G111	2.11	
	G112–G116	2.69	
	G117–G120	4.76	
77	G11–G18	3.58	31.009
	G19–G111	2.11	
	G112–G116	2.68	
	G117–G120	4.79	
78	G11–G18	3.55	30.998
	G19–G111	2.09	
	G112–G116	2.67	
	G117–G120	4.82	
79	G11–G18	3.51	30.998
	G19–G111	2.06	
	G112–G116	2.67	
	G117–G120	4.85	
80	G11–G18	3.46	30.698
	G19–G111	2.00	
	G112–G116	2.67	
	G117–G120	4.90	
81	G11–G18	3.43	30.589
	G19–G111	1.94	
	G112–G116	2.67	
	G117–G120	4.94	
82	G11–G18	3.41	30.458
	G19–G111	1.85	
	G112–G116	2.68	
	G117–G120	4.99	

Table A1. *Cont.*

Water Cut, %	Layer-Segment Combination	Seepage Resistance Gradient	Stage Recovery Rate, %
83	G11–G18	3.39	30.289
	G19–G111	1.77	
	G112–G117	4.83	
	G118–G120	4.76	
84	G11–G18	3.40	30.103
	G19–G111	1.76	
	G112–G117	4.83	
	G118–G120	4.76	
85	G11–G18	3.39	29.876
	G19–G111	1.80	
	G112–G117	4.82	
	G118–G120	4.77	
86	G11–G18	3.40	29.654
	G19–G111	1.88	
	G112–G117	4.79	
	G118–G120	4.78	
87	G11–G18	3.40	29.345
	G19–G111	1.95	
	G112–G117	4.74	
	G118–G120	4.80	
88	G11–G18	3.41	29.223
	G19–G111	1.98	
	G112–G117	4.77	
	G118–G120	4.81	
89	G11–G18	3.42	29.101
	G19–G111	2.00	
	G112–G117	4.85	
	G118–G120	4.83	
90	G11–G18	3.42	28.765
	G19–G111	2.01	
	G112–G117	4.93	
	G118–G120	4.86	
91	G11–G18	3.42	28.469
	G19–G114	3.53	
	G115–G117	4.00	
	G118–G120	4.89	
92	G11–G18	3.40	28.324
	G19–G114	3.63	
	G115–G117	4.01	
	G118–G120	4.94	
93	G11–G18	3.37	28.208
	G19–G114	3.70	
	G115–G117	4.01	
	G118–G120	5.01	
94	G11–G18	3.33	28.134
	G19–G114	3.75	
	G115–G117	4.00	
	G118–G120	5.08	
95	G11–G18	3.31	28.130
	G19–G114	3.84	
	G115–G117	3.99	
	G118–G120	5.14	

Table A1. *Cont.*

Water Cut, %	Layer-Segment Combination	Seepage Resistance Gradient	Stage Recovery Rate, %
96	G11–G18	3.30	28.120
	G19–G114	3.97	
	G115–G117	3.99	
	G118–G120	5.17	
97	G11–G18	3.28	28.100
	G19–G114	4.12	
	G115–G117	4.04	
	G118–G120	5.20	

Appendix B

Taking layered water injection starting from a moisture content of 70% as an example, the specific cost analysis data can be found in Table A2.

Table A2. Economic parameter data.

Initial Investment			Operation and Maintenance Costs (Project Operating Cycle of 20 Years)		
Layered Water Injection System Device	**Software Development Cost**	**System Integration and Adjustment**	**Data Monitoring and Analysis**	**Equipment Maintenance and Updates**	**Total Annual Operating Costs**
CNY 500,000 per well	CNY 500,000	CNY 200,000	CNY 200,000 per year	CNY 100,000 per year	CNY 300,000 per year
Oil price	Discount rate	Management fee		Safety production cost	
2969 CNY/ton	8%	400 CNY/ton		20 CNY/ton	

$$\text{Initial investment} = 500{,}000 \times 6 + 500{,}000 + 200{,}000 = \text{CNY } 3{,}700{,}000$$

$$\text{Operation and maintenance costs} = (200{,}000 + 100{,}000 + 300{,}000) \times 20 = \text{CNY } 1{,}200{,}000$$

$$\text{Total initial investment} = 3{,}700{,}000 + 1{,}200{,}000 = \text{CNY } 4{,}900{,}000$$

The geological reserves of crude oil in Block D are about 1.8×10^6 ton, and the oil recovery rate has been improved by 3.97%.

$$\text{Additional crude oil production} = 1.8 \times 10^6 \times 3.97\% = 71{,}460 \text{ ton}$$

$$\text{Extra income} = 71{,}460 \times 2969 = \text{CNY } 212{,}160{,}000$$

$$\text{Management fee and safety production fee} = (400 + 20) \times 71{,}460 = \text{CNY } 30{,}010{,}000$$

$$\text{Total benefit} = 212{,}160{,}000 - 30{,}010{,}000 = \text{CNY } 182{,}150{,}000$$

Calculate net present value (NPV), where t is the project running cycle:

$$\text{NPV} = \sum_{t=1}^{20} \frac{\text{Total benefit}}{(1+0.08)^t} - \text{Total initial investment}$$

The calculated NPV is approximately CNY 34.188 million, and the net present value is much greater than 0, indicating that this scheme has high economic efficiency.

Conduct sensitivity analysis to evaluate the impact of uncertainty.

Crude oil price fluctuations: If the oil price drops by 20%, the additional revenue will decrease to CNY 169.73 million, and the NPV will still be about CNY 25.083 million, indicating that the plan is still profitable.

Cost overrun: If the initial investment increases by 50%, the total cost will be CNY 7.35 million, but the NPV will still be as high as CNY 31.738 million, and the economy will not be significantly affected.

The increase in recovery rate: If the recovery rate only increases by 2%, the additional income will be CNY 106.88 million, and the NPV will still be about CNY 11.596 million. The project is still feasible.

Economic benefit analysis shows that the fine water injection interval dynamic control method based on seepage resistance has significant economic feasibility in the application of D block.

References

1. Wang, D.; Liu, F.; Li, G.; He, S.; Song, K.; Zhang, J. Characterization and Dynamic Adjustment of the Flow Field during the Late Stage of Waterflooding in Strongly Heterogeneous Reservoirs. *Energies* **2023**, *16*, 831. [CrossRef]
2. Anderson, W.G. Wettability Literature Survey Part 5: The Effects of Wettability on Relative Permeability. *J. Pet. Technol.* **1987**, *39*, 1453–1468. [CrossRef]
3. Jiang, R.; Qiao, X.; Teng, W.; Xu, J.; Sun, S.; Xie, L. Impact of physical properties time variation on waterflooding reservoir development. *Fault-Block Oil Gas Field* **2016**, *23*, 768–771. Available online: https://www.dkyqt.com/#/digest?ArticleID=3774 (accessed on 13 November 2025).
4. Spooner, V.E.; Geiger, S.; Arnold, D. Dual-porosity flow diagnostics for spontaneous imbibition in naturally fractured reservoirs. *Water Resour. Res.* **2021**, *57*, e2020WR027775. [CrossRef]
5. Victoria, S.; Sebastian, G.; Arnold, D. Ranking Fractured Reservoir Models Using Flow Diagnostics. In Proceedings of the SPE Reservoir Simulation Conference, Galveston, TX, USA, 10–12 April 2019. [CrossRef]
6. Willis, B.J.; Sech, R.P. Quantifying Impacts of Fluvial Intra-Channel-Belt Heterogeneity on Reservoir Behaviour. In *Fluvial Meanders and Their Sedimentary Products in the Rock Record*; Ghinassi, M., Colombera, L., Mountney, N.P., Reesink, A.J.H., Bateman, M., Eds.; John Wiley & Sons: Hoboken, NJ, USA, 2018. [CrossRef]
7. Baker, R.O.; Kuppe, F.; Chugh, S.; Bora, R.; Stojanovic, S.; Batycky, R. Full-Field Modeling Using Streamline-Based Simulation: Four Case Studies. *SPE Reserv. Eval. Eng.* **2002**, *5*, 126–134. [CrossRef]
8. Datta-Gupta, A. Streamline Simulation: A Technology Update (includes associated papers 71204 and 71764). *J. Pet. Technol.* **2000**, *52*, 68–84. [CrossRef]
9. Batycky, R.P.; Thiele, M.R. Technology Update: Mature Flood Surveillance Using Streamlines. *J. Pet. Technol.* **2016**, *68*, 22–25. [CrossRef]
10. Chen, H.; Park, J.; Datta-Gupta, A.; Shekhar, S.; Grover, K.; Das, J.; Shankar, V.; Kumar, M.S.; Chitale, A. Improving Polymerflood Performance Via Streamline-Based Rate Optimization: Mangala Field, India. In Proceedings of the SPE Improved Oil Recovery Conference, Virtual, 31 August–4 September 2020. [CrossRef]
11. Thiele, M.R.; Batycky, R.P. Using Streamline-Derived Injection Efficiencies for Improved Waterflood Management. *SPE Reserv. Eval. Eng.* **2006**, *9*, 187–196. [CrossRef]
12. Jia, H.; Deng, L. Water flooding flowing area identification for oil reservoirs based on the method of streamline clustering artificial intelligence. *Pet. Explor. Dev.* **2018**, *45*, 328–335. [CrossRef]
13. Tanaka, S.; Onishi, T.; Kam, D.; Dehghani, K.; Wen, X.-H. Application of Combined Streamline Based Reduced-Physics Surrogate and Response Surface Method for Field Development Optimization. In Proceedings of the International Petroleum Technology Conference, Dhahran, Saudi Arabia, 13–15 January 2020. [CrossRef]
14. Zhao, C.; Kong, X.; Shi, L.; Zhang, Z.; Zhang, C. Numerical Simulation Study on Factors Affecting Water-Flooding Efficiency. *Contemp. Chem. Ind.* **2016**, *45*, 1640–1642+1646. [CrossRef]
15. Zhang, B. Study on Numerical Simulation of Reservoir Fine Water Injection Development Considering Reservoir Heterogeneity. *Int. J. Energy* **2025**, *6*, 65–68. [CrossRef]
16. Wang, F.; Xu, D.; Yu, L.; Zhang, F.; Liu, C.; Zhen, K. The Full-Automatic Real-Time Display, Testing and Adjustable System in Separated Layers Water Injection Well. In Proceedings of the SPE Intelligent Energy International, Utrecht, The Netherlands, 27–29 March 2012. [CrossRef]
17. Sun, F.; Jia, D.; Yu, J.; Pei, X.; Liu, H.; Zheng, L.; Shujun, B.A. Separate Layer Water Injection for Offshore Directional Wells. In Proceedings of the SPE Asia Pacific Oil & Gas Conference and Exhibition, Perth, Australia, 25–27 October 2016. [CrossRef]

18. Song, Z.; Liu, Y.; Yang, J.; Zhou, H.; Feng, G.; Huo, L.; Wang, Y.; Zhang, Y.; Cao, X.; Liu, B.; et al. Application of Remote Monitoring and Controlling Intelligent Separated Layer Water Injection Technology in BQ Oilfield, Dagang. In Proceedings of the International Petroleum Technology Conference, Dhahran, Saudi Arabia, 12–14 February 2024. [CrossRef]
19. Guo, J.; Yang, E.; Zhao, Y.; Fu, H.; Dong, C.; Du, Q.; Zheng, X.; Wang, Z.; Yang, B.; Zhu, J. A New Method for Optimizing Water-Flooding Strategies in Multi-Layer Sandstone Reservoirs. *Energies* **2024**, *17*, 1828. [CrossRef]
20. Du, Q. Variation law and microscopic mechanism of reservoir permeability in sandstone oilfields by long-term water flooding. *Acta Pet. Sin.* **2016**, *37*, 1159–1164. [CrossRef]
21. Huang, B.; Xu, R.; Fu, C.; Zhang, W.; Shi, Z. Multi-level fuzzy identification method for interwell thief zone. *Lithol. Reserv.* **2018**, *30*, 105–112. Available online: https://kns.cnki.net/kcms2/article/abstract?v=7DUETwKSFy4IBT6fyDUNF-ezFTCv1Q4kKtXjUwyzQwvMy-kFJ6CQ0NQ-OvIKDSo29Umz4uW_lDZD34FOa_eleq65k_1wlgKiircCj18v-uFeB9mxz-O3tB2HdKsSR3u-eUJMOylcbnUqTO4K1mq185dnMoxFVkbe7xQTKrl0q-5ELEGN43Kv1g==&uniplatform=NZKPT&language=CHS (accessed on 13 November 2025).
22. Shan, G.; Wang, C.; Wang, Z.; Jiang, X.; Guo, J. Water Injection Adjustment Method Based on Dynamic Flow Resistance. *Xinjiang Pet. Geol.* **2023**, *44*, 435–441. [CrossRef]
23. Luo, X.; Peng, B. Classification and Management Method for Non-productive Circulation Based on Seepage Resistance. Xi'an Petroleum University, Shaanxi Petroleum Society. In Proceedings of the 2019 International Conference on Oil and Gas Field Exploration and Development; Geological Brigade, Fourth Oil Production Plant, Daqing Oilfield, Xian, China, 16–18 October 2019; pp. 1781–1787. [CrossRef]
24. Gao, W.; Yin, R.; Gao, N.; Sheng, H.; Gao, Z. Establishment and Application of a New Analytical Fractional Flow Equation. *Xinjiang Pet. Geol.* **2021**, *42*, 179–187. [CrossRef]
25. Zhang, L.; Tian, P.; Ren, Y.; Yin, Y.; Xing, C.; Lu, X. Optimization of Water Injection Pressure for Water-Flood Development in Offshore Oilfields. *Xinjiang Pet. Geol.* **2021**, *42*, 63–67. [CrossRef]

Disclaimer/Publisher's Note: The statements, opinions and data contained in all publications are solely those of the individual author(s) and contributor(s) and not of MDPI and/or the editor(s). MDPI and/or the editor(s) disclaim responsibility for any injury to people or property resulting from any ideas, methods, instructions or products referred to in the content.